Mini Quadrotor UAV: Design and Experiment

Elisa Capello[1]; Alessandro Scola[2]; Giorgio Guglieri[3]; and Fulvia Quagliotti[4]

Abstract: The purpose of this work is to design a new layout for a quadrotor unmanned aerial vehicle (UAV) for experimental customized control-system validation. Geometrical and structural properties have been computed, and commercial off-the-shelf equipment has been selected. The flight control system, both hardware and software, has been custom developed; the same applies for the mathematical model describing the flight dynamics. Two proportional-derivative (PD) controllers have been designed and experimentally tested. A different control strategy with a state feedback controller has been implemented, assigning a robust eigenstructure and the desired dynamic specifications. An adaptive algorithm, which guarantees a uniformly bounded response for both the inputs and the outputs, has been presented. An L1 adaptive controller has been studied and implemented, including the state predictor and the adaptive and control laws. Tests with the PD controller have shown slowly stable response even in the event of numerical and vibrational noise. In conclusion, the L1 adaptive controller permits one to obtain optimal response characteristics, and the low-pass filter integrated in control law, combined with a Kalman filter, can reduce noise and correlate data between different sensors. **DOI: 10.1061/(ASCE)AS.1943-5525.0000171.**

CE Database subject headings: Control systems; Experimentation; Design; Aerospace engineering; Probe instruments.

Author keywords: Quadrotor UAV; Customized control board; L1 adaptive controller; Experimental model.

Introduction

In the last few years, small unmanned aerial vehicles (UAVs) have been developed for large-scale territorial monitoring. The commercial and civilian sectors have expressed an interest in small vertical take-off and landing (VTOL) vehicles capable of reducing take-off and landing distance, to fly over a target and complete many tasks, without the need for excess pilot workload or risk of life. For this reason, small rotary-wing UAVs have been the subject of several recent research projects. Because of the complexity in control and the intrinsic dynamics of these small-size vehicles, multirotor unmanned vehicles have been developed (Guernard et al. 2005; McKerrow 2004; Castillo et al. 2004; Pounds et al. 2002).

Small quadrotors have many potential missions including indoor flight and operations in urban areas. A quadrotor might achieve stable hovering and precise flight by balancing the forces produced by the four rotors. However, the onboard software will have to fit in the available memory of the small microprocessors but be powerful enough to provide control with sensor data of limited quality.

A quadrotor has four motors located at the front, rear, left, and right ends of a cross frame. The quadrotor is controlled by changing the speed of rotation of each motor. The front and rear rotors rotate in a direction, e.g., counterclockwise, while the left and right rotors rotate in the opposite direction, to balance the torque created by the spinning rotors. The relative speed of the front and rear rotors is varied to control the pitch rate of the UAV. Increasing the speed of the front motor by the same amount that the speed of the rear one is decreased will keep the total thrust provided by the four rotors constant. Furthermore, the total torque created by these two rotors will remain constant. Similarly, the roll rate is controlled by varying the relative speed of the left and right rotors. The yaw rate is controlled by varying the relative speed of the clockwise (right and left) and counterclockwise (front and rear) rotors. The collective thrust is controlled by varying the speed of all the rotors simultaneously.

The Aerospace Engineering Department of Politecnico di Torino is working on the development of a quadrotor used primarily as a test bed for customized control algorithms. Moreover, its commercial purpose is territorial monitoring and multirole missions (Capello et al. 2009). The research is oriented to analyze stability and control issues for this platform.

Before a prototype is available for experiments, a working mathematical model reproducing as accurately as possible the dynamic in-flight behavior is required to assess the layout of the configuration, the performances, the stability, and the response to controls. Another concern is the design of control laws for assisted remote piloting or fully autonomous flight.

The paper is organized in the following way. In the Onboard Controller section, the onboard controller is described with regard to the flight tests. The Mathematical Model section describes the complete and experimental mathematical model. In the Simulation Results and Experimental Flight Tests section, the simulation and experimental results are outlined. In the Dynamic Analysis and Eigenstructure Assignment section, the dynamic analysis is presented with

[1]Graduate Research Assistant, Aerospace Engineering Dept., Politecnico di Torino, Corso Duca degli Abruzzi 24, 10129 Turin, Italy (corresponding author). E-mail: elisa.capello@polito.it

[2]Former Graduate Research Assistant, Aerospace Engineering Dept., Politecnico di Torino, Corso Duca degli Abruzzi 24, 10129 Turin, Italy. E-mail: alessandro.scola@polito.it

[3]Associate Professor, Aerospace Engineering Dept., Politecnico di Torino, Corso Duca degli Abruzzi 24, 10129 Turin, Italy. E-mail: giorgio.guglieri@polito.it

[4]Associate Professor, Aerospace Engineering Dept., Politecnico di Torino, Corso Duca degli Abruzzi 24, 10129 Turin, Italy. E-mail: fulvia.quagliotti@polito.it

Note. This manuscript was submitted on February 18, 2011; approved on September 30, 2011; published online on September 14, 2012. Discussion period open until March 1, 2013; separate discussions must be submitted for individual papers. This paper is part of the ***Journal of Aerospace Engineering***, Vol. 25, No. 4, October 1, 2012. ©ASCE, ISSN 0893-1321/2012/4-559–573/$25.00.

regard to the applied eigenstructure. The L1 Adaptive Controller section presents the L1 adaptive control. The Conclusion section summarizes the results.

Onboard Controller

The quadrotor flight control has been assigned to the onboard controller.

This controller is needed for two reasons:

- To mix the command signals received from the on-board receiver. These input signals are sent by a ground operator with a remote controller, moving the stick to perform the requested maneuver.
- To perform the feedback control and to enforce a stable flight or maintain a desired attitude and position, if these characteristics are implemented.

A commercial off-the-shelf controller board has been sought out. The principal drawback of a commercial board is related to the inability to modify the control algorithm implemented on the board and to know exactly how the controller works. Because of this, a custom-made controller has been designed and produced. The board is designed to research the following:

- Flight testing of different feedback control laws,
- Autonomous flight mode, and
- Formation flight.

The first board is designed to perform some basic functions. In Fig. 1 the functional scheme is shown as scheduled initially. To obtain the desired flight parameters, a three-axis accelerometer and a single-axis gyroscope are used.

From the accelerometers, the pitch and bank angles are derived using the classical equations of dynamics for a rigid body (Pamadi 2004; Etkin and Reid 1995). A single-axis gyroscope is needed to measure the yaw rate, making possible the computation of the yaw Euler angle rate, using the kinematic equation

$$\dot{\psi} = q \sin \Phi / \cos\Theta + r \cos \Phi / \cos\Theta \tag{1}$$

Therefore, the control board has the ability to perform the aforementioned computation and to manage different-channel signals as inputs from the receiver, the accelerometers, and the gyroscope, and it can perform the feedback function.

As shown in Fig. 1, the feedback acts on the Euler angles and on the pitch and roll rates to maintain the desired attitude; in the development phase the hover condition is chosen as a reference. The output feedback signals are added to the pilot command, and the so-composed signals increase or decrease the motor rotational speed.

In the first version of the controller board, currently installed on the platform, the gyroscope did not perform as expected; thus it was removed, neglecting the influence of the yaw rate and the yaw Euler angle. The error introduced is minimal, considering that the quadrotor is hovering; thus the perturbations in attitude angle and angular velocity have to be limited. Usually, the contribution of the yaw angular rate is smaller than the pitch and roll angular terms.

The board feedback is a proportional-derivative (PD) controller; it has been decided to start with this controller because of its well-known modus operandi. The controller variation is made by updating the firmware, and the next step will be the implementation of a new control law, that is, an L1 adaptive controller.

The feedback gains can be modified through specifically developed software, the interface of which is shown in Fig. 2. The input IN_i are the signals from the transmitter, and the output OUT_i are the angular velocities of each of the motors Ω_i. The input range consists of pulse-width modulation signals (mean value 1.5 ms).

The left matrix correlates inputs and outputs, whereas the right one embodies the feedback gains. Thus, the output commands are a mix between the transmitter signals and the control feedback ones.

Moreover, the software allows the attitude angles, the angular rates, and the acceleration along the three axes to be seen in real time, from which angles and rates are derived.

However, during the experimental activity, some noise was measured in the signals because of structural vibrations and the numerical elaboration. For example, the trend of the angular rates, obtained by deriving angles, contains some fluctuating disturbances and random glitches. To reduce this noise the derivatives of the angles have been calculated with a second-order finite-difference formula, but this method is not sufficient to obtain clean signals.

Therefore, a completely new controller board has been designed. To accomplish the goal of a stable flight, the use of commercially available hardware is emphasized, and the design is made as simple as possible. The microcontroller and micro electro-mechanical system sensors are both lightweight and low cost. The new layout is given in Fig. 3.

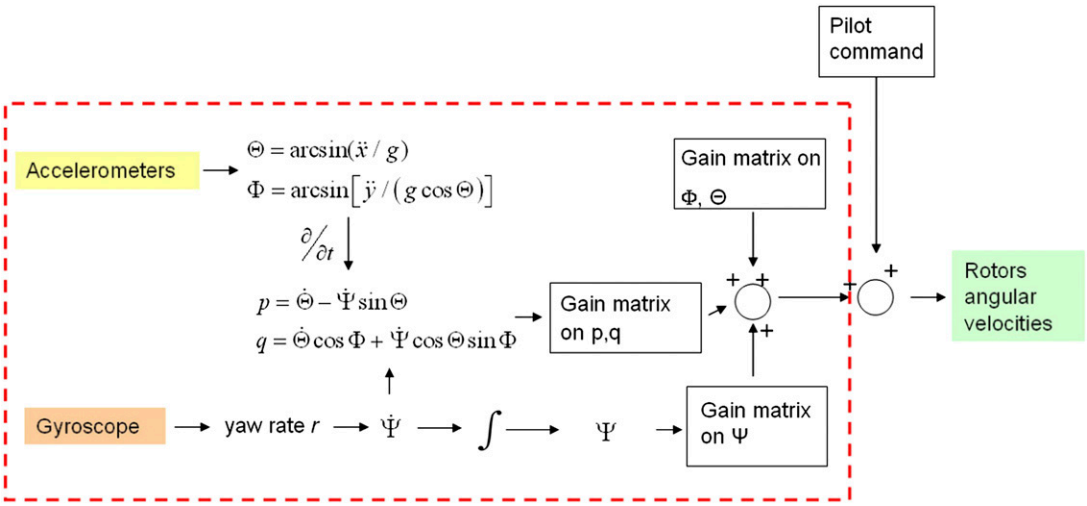

Fig. 1. Controller-board functional scheme as scheduled initially

J. Aerosp. Eng. 2012.25:559-573.

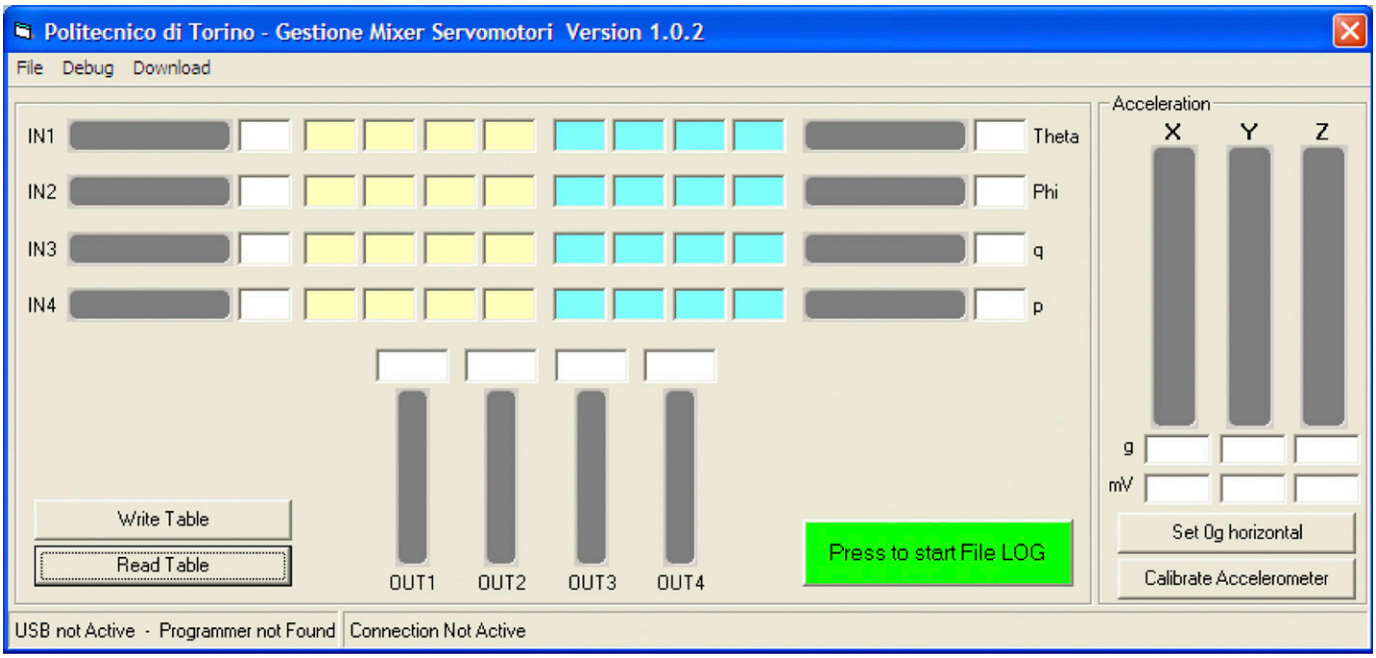

Fig. 2. Motor-management-software interface

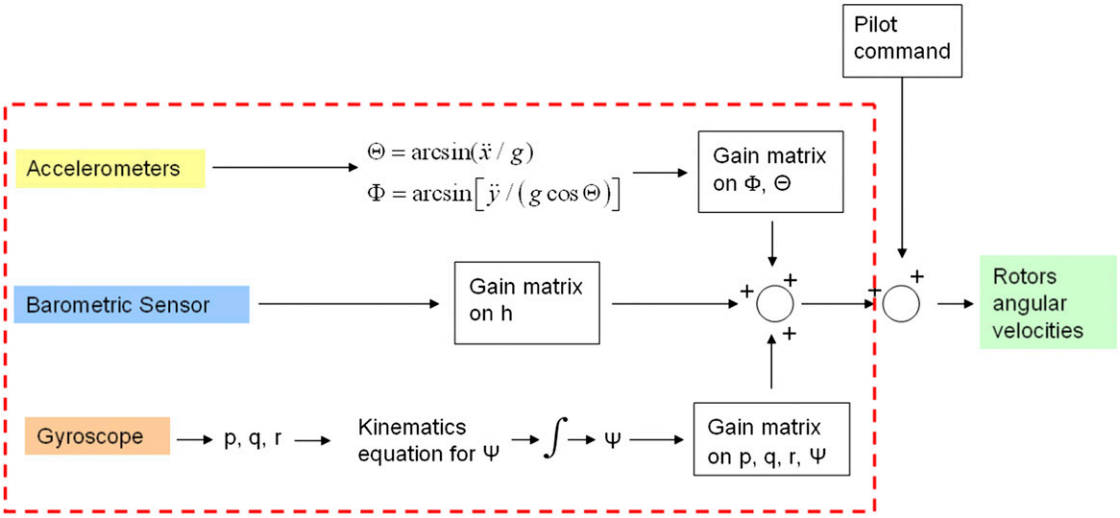

Fig. 3. New layout of controller-board functional scheme

A three-axis gyroscope has been installed, replacing the single-axis one; thus all the angular rates are now measured directly, avoiding or at least reducing the noise originated by numerical derivation of attitude angles, calculated from the accelerometers. However, this signal is contaminated by random fluctuations or by high-frequency noise; thus it may be best to integrate it using the trapezoid rule (Lynn and Fuerst 1995).

Furthermore, a barometric sensor has been integrated to perform feedback on altitude, obtaining an altitude-hold system.

The gyroscope measurements can be used to provide good feedback control of the inner control loop; in practice, it is easily obtained if a filter is implemented to cancel the sensor bias. Accurate angle measurements are more difficult to obtain. In fact the angle estimate depends largely on the direct integration of the angular rates. The authors have verified that if a filter and a feedback on the determination of the Euler angles are included in the last version of the controller board, a pilot is able to command the quadrotor to lift off the ground, fly above a small area, and land.

Because of measurement problems and sensor bias, a filter is required. Thus, a future work is the implementation of a Kalman filter to obtain a fusion of the data from both the accelerometer and gyroscope.

Mathematical Model

The analysis of photogrammetric applications, considering the platform characteristics, can be performed with an L1 mathematical model, sufficient to define the reference-simulation model. The L1 model (Table 1) defines the conventional six-degree-of-freedom

J. Aerosp. Eng. 2012.25:559-573.

Table 1. Levels of Rotor Mathematical Modeling

	Level 1	Level 2	Level 3
Aerodynamics	Linear 2D Dynamic inflow Momentum theory	Nonlinear (limited 3D) Dynamic inflow Momentum theory Local effects of blade Unsteady 2D Compressibility	Nonlinear 3D Full wake analysis Unsteady 2D Compressibility
Dynamics	Rigid blades	Rigid blades as in L1	Detailed structural representation as elastic modes or finite-element rotor design
	Quasi-steady motion	Limited number of blade elastic modes	
Applications	Parametric trends for flying qualities and performance studies within operational flight envelope	Parametric trends for flying qualities and performance studies up to operational flight envelope	Rotor limit load prediction
	Low-bandwidth control	Medium bandwidth appropriate to high-gain active flight control	Vibration analysis Rotor stability analysis up to safe-flight envelope

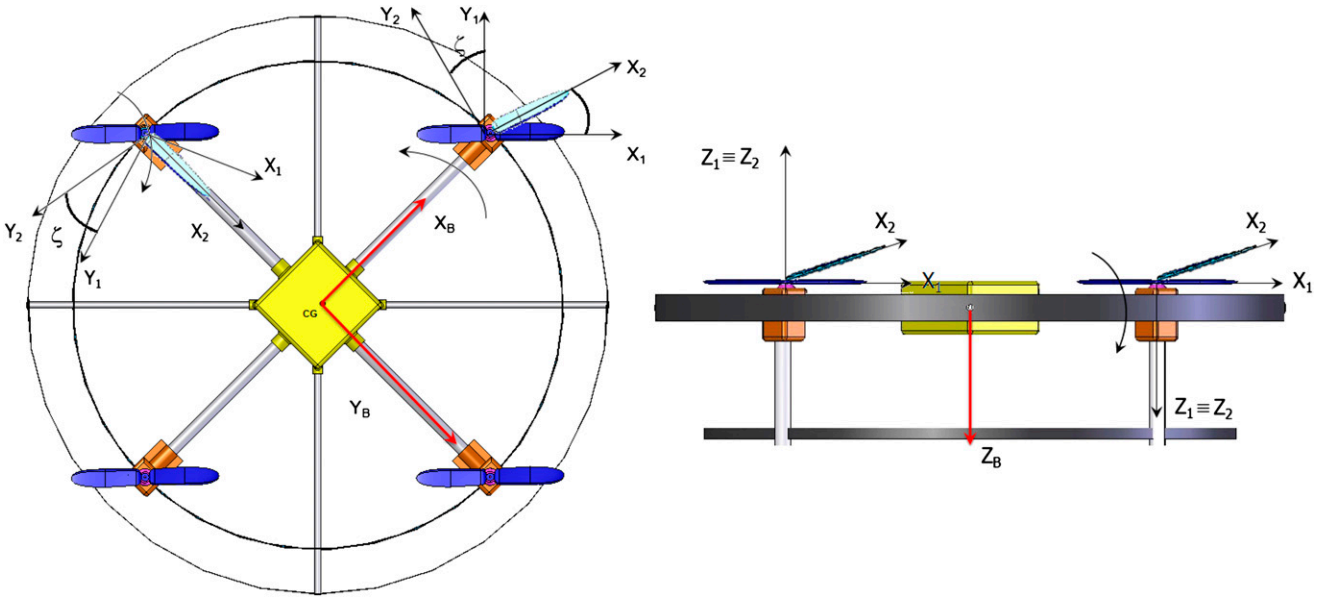

Fig. 4. Reference frames for the development of mathematical model; the body axis frame used to write the equations of motion is represented by the subscript B

flight-mechanics formulation for the fuselage and the rotor dynamics considered as a disc with coning and tilting displacements. Unsteady (frequency-dependent) aerodynamic effects are ignored. The L1 complexity aims to describe the key features of the flight. This type of simplified model reproduces the real vehicle with bounded discrepancy limited to 20% of the state changes (Padfield 2007).

To obtain the forces and moments acting on the platform, as for a conventional helicopter (Pamadi 2004), different reference frames have to be defined. Some of these are visible in Fig. 4. The complete mathematical model, considering the rotors and the fuselage, is written in the body reference frame.

Each blade is modeled as a thin bar with uniform mass distribution along its radius. The variation of blade section twist is linear. No feathering hinge is modeled, as the blade operates with fixed pitch settings.

Forces and moments have been computed in the most convenient reference frame, which is subsequently transformed into the body axis frame. Many axis systems are needed, as there is not a single axis system suitable for specifying all forces, moments, velocities, and accelerations (Pamadi 2004). That is why it was necessary to define seven reference frames (in Fig. 4 only five of them are visible for the sake of clarity). Details for the mathematical model can be found in (Pamadi 2004; Prouty 2005; Stevens and Lewis 2003; Johnson 1994).

In reference frame F_2 the origin is in the center of the propeller hub, rotating with the blades, with the x-axis running from hub to tip, the y-axis 90° advanced with respect to the x-axis, and the z-axis forming a right-handed system. The F_1 frame is hub centered and rotates with the blades, so it is called the partially rotating frame. Clearly, the F_1 and F_2 frames differ between clockwise and counterclockwise propellers.

The nonrotating frame is again hub centered but does not rotate; the north-east-down frame is in the platform center of gravity (as the body axis frame). This latter frame is presented in Fig. 4.

The propeller blades have constant flap angle β and lag angle ζ. A final assumption provides that blades always work far from stall conditions, so a coefficient of lift–angle-of-attack linear dependency exists.

J. Aerosp. Eng. 2012.25:559-573.

Starting from the helicopter theory, some simplifications can be adopted knowing the platform characteristics. The attention is focused on the evaluation of the mathematical model for clockwise rotors. The equations of motion of a helicopter are written for a counterclockwise rotor, and if a clockwise one is considered, a negative value of the rotational speed is implemented in the equations of motion. In fact (in the literature) the helicopter equations of motion presented have been detailed for counterclockwise rotors. In this paper, the clockwise equations are also analyzed.

Each blade is affected by the airflow because of the combination of the rotational speed, the forward speed of the vehicle, and the inflow attributable to blade lift. (Flap and lag dynamics are neglected on account of the hypothesis of constant flap and lag angles.) Inflow dynamics are modeled as uniform, and the twist is assumed linear.

Moreover, even when moving in forward flight the quadrotor passes through hover states, being the real phases of translational flights limited to short transition; for the same reason, the fuselage drag and the propeller angular rate have been neglected.

The rotation angles between F_1 and F_2 are the coning β and the lag ζ; the F_2 frame is useful to compute forces and moments acting on the blades. The coordinate transformation matrix is

$$[R]_{2c}^{1} = [R]_{\beta}[R]_{\zeta} = \begin{bmatrix} \cos\beta\cos\zeta & -\cos\beta\sin\zeta & \sin\beta \\ \sin\zeta & \cos\zeta & 0 \\ -\sin\beta\cos\zeta & \sin\beta\sin\zeta & \cos\beta \end{bmatrix} \tag{2}$$

where subscript c identifies the matrix for clockwise-turning propellers.

The matrix between the body frame F_B and the partially rotating frame F_1 is

$$[R]_{1c}^{B} = \begin{bmatrix} -\cos\Psi & \sin\Psi & 0 \\ \sin\Psi & \cos\Psi & 0 \\ 0 & 0 & -1 \end{bmatrix} \tag{3}$$

where ψ = azimuth of the blade.

Initially, the loads acting on the blades, both aerodynamic and inertial ones, were computed using the classical method adopted for helicopters (Padfield 2007); that is, the loads were calculated at each revolution of the propellers by integrating both along the blade radius and azimuth angle. Later this approach was dropped in the equations of motion because of its complexity for simulation in real time. Considering the platform characteristics, i.e., constant flap and lag, the loads are computed for different propeller rotation speeds.

Inertial Forces and Moments Acting on Blades

Infinitesimal inertial forces F^i and moments M^i, acting on a segment of the blade, have been computed using

$$dF^i = -dm \cdot a_p^i \tag{4}$$

$$dM^i = -r_0 \cdot dm \cdot a_p^i \tag{5}$$

where dm = infinitesimal mass, a_p = acceleration, and r_0 = moment arm.

Aerodynamic Forces and Moments Acting on Blades

Lift and drag have been calculated on an infinitesimal strip of the blade using

$$dL = 1/2\,\rho U_0^2 C_L\, dS \tag{6}$$

$$dD = 1/2\,\rho U_0^2 C_D\, dS \tag{7}$$

where ρ = air density, c = blade mean aerodynamic chord, R = radius, U_0 = air speed, C_L and C_D = lift and drag coefficients of the blade airfoil, and dx = width of a nondimensional blade infinitesimal strip. Within these assumptions, C_L is linearly dependent on the angle of attack, and C_D is a quadratic function of lift.

The forces and moments for clockwise propellers are given in Fig. 5, taking into account that for counterclockwise propellers different transformation matrices are required. The velocity U_0 is given in the reference frame F_1:

- The speed was computed,
- This speed was substituted in Eqs. (6) and (7), and
- The infinitesimal lift and drag were transformed along reference frame F_2 and were integrated along the blade.

The final relationships, as an example of aerodynamic forces along the y_2-axis, became

$$F_{Y2}^{A} = -1/2\rho cRU_0^2\left[\int_0^1 \sin\chi C_L dx + \int_0^1 \cos\chi C_D dx\right] \tag{8}$$

where χ = aerodynamic angle between U_0 and Y_2.

The speed is obtained by the superposition of three velocities: the blade speed, because of its rotational motion; the quadrotor forward speed, which is zero in hovering; and the propeller-induced inflow. It is noteworthy that Eq. (8) contains both time- and space-dependent terms correlated by the blade azimuth position Ψ.

An analytical solution was investigated to calculate the aerodynamic forces and moments, as reported in Eq. (8). To reduce the computational time and simplify the complete model, the aerodynamic loads were calculated using the Taylor-series expansions of the equations (small angles of attack were considered), for different propeller angular rates.

This approach has been useful to evaluate the magnitude of the aerodynamic forces and moments with respect to the F_2 frame. The only nonnegligible aerodynamic loads are acting along the Z axis, i.e., the thrust and the reaction torque. This is verified by applying the method presented in (Flachsbart and Krober 1929), and subsequently, torque and force varying with propeller rotation speed were measured experimentally.

The graphs in Figs. 6 and 7 show torque and thrust plotted against Ω measured experimentally and subsequently used in the mathematical model.

Equations of Motion

The equations of motion written with respect to the body reference frame are reported in Eqs. (9)–(14). The inertial tensor is diagonal because of the quadrotor symmetry, and the drag of structure has been neglected when the quadrotor is in forward flight. Thus, the loads acting are the thrust, the reaction torque, and the weight.

To complete the mathematical model the kinematic equations to describe the Euler-angle rate (Pamadi 2004; Etkin and Reid 1995) have to be included, compliant with the classical mechanical assumptions

$$\dot{u} = vr - wq + g\sin\Theta \tag{9}$$

$$\dot{v} = wp - ur + g\cos\Theta\sin\Phi \tag{10}$$

$$\dot{w} = uq - vp + g\cos\Phi\cos\Theta - \frac{T_1 + T_2 + T_3 + T_4}{m} \tag{11}$$

J. Aerosp. Eng. 2012.25:559-573.

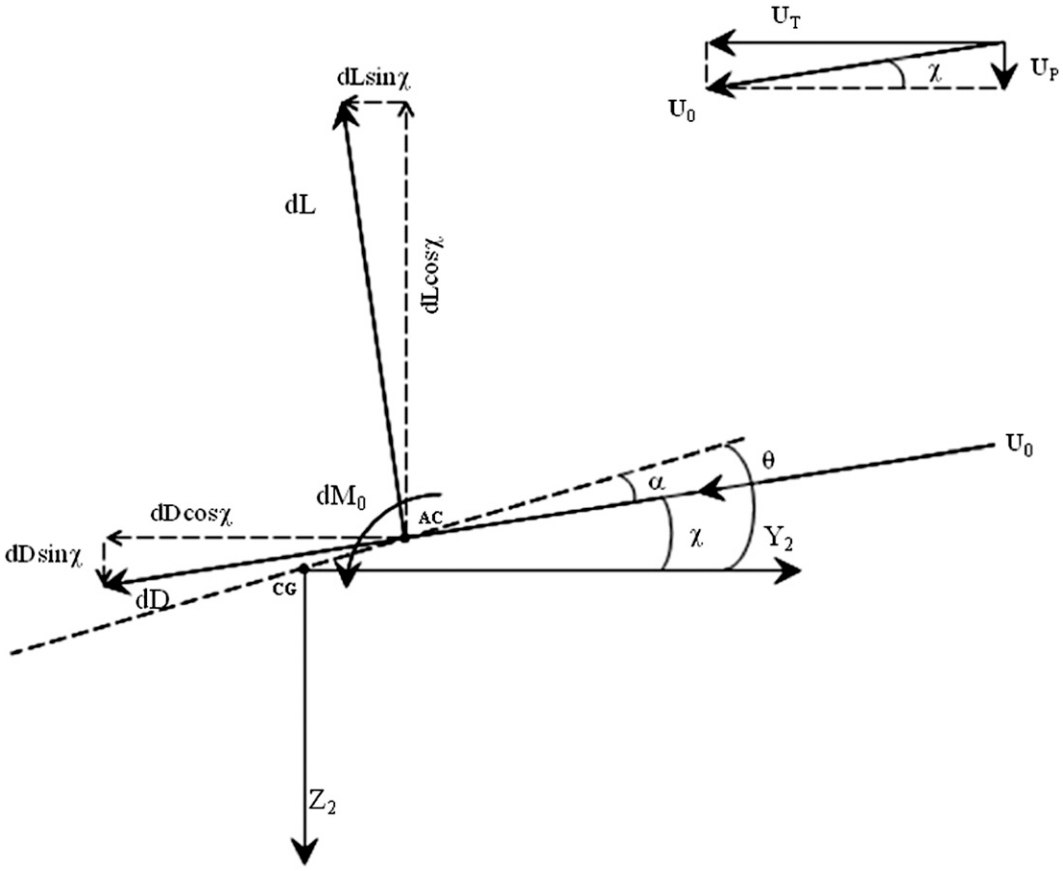

Fig. 5. Forces and moments on the clockwise-rotating blades

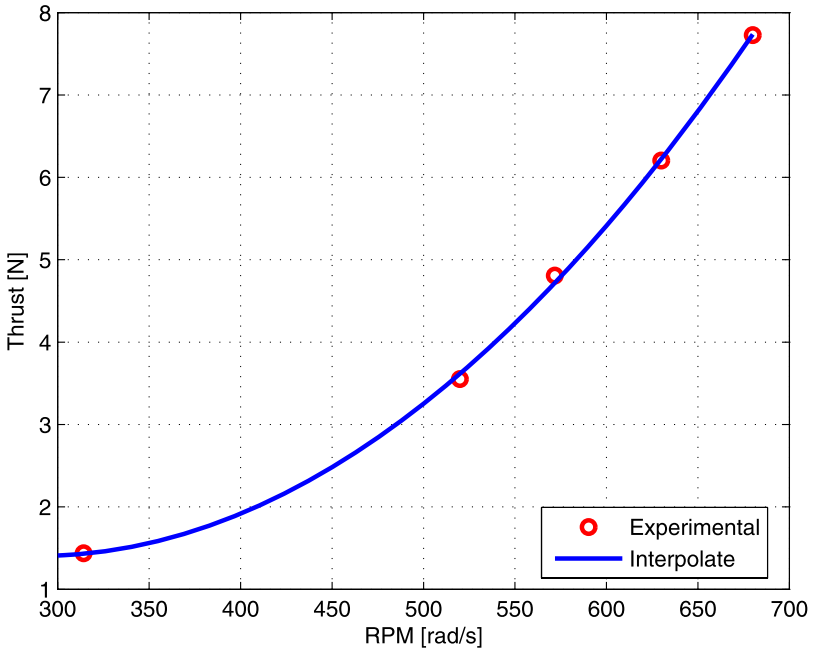

Fig. 6. Thrust versus propeller rotation speed

J. Aerosp. Eng. 2012.25:559-573.

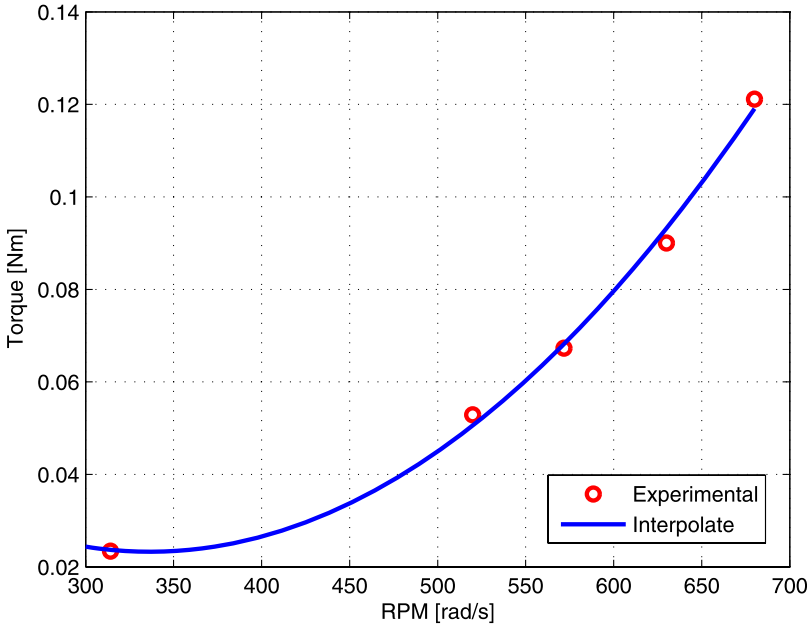

Fig. 7. Torque versus propeller rotation speed

$$\dot{p} = \frac{1}{I_X}\left[(T_2 - T_4)\frac{d}{2} - qr(I_Z - I_Y) - J_P q\Omega\right] \tag{12}$$

$$\dot{q} = \frac{1}{I_Y}\left[(T_1 - T_3)\frac{d}{2} - pr(I_X - I_Z) + J_P p\Omega\right] \tag{13}$$

$$\dot{r} = \frac{1}{I_Z}[(C_1 - C_2 + C_3 - C_4) - pq(I_Y - I_X)] \tag{14}$$

where u, v, w = linear velocities, m = quadrotor mass, T_i = ith motor thrusts, C_i = ith motor reaction torques, I_X, I_Y, I_Z = moment of inertia with respect to the body axes, d = distance between each motor and the quadrotor center of gravity, J_P = moment of inertia about the propeller axis, and Ω = propeller rotational speed. Note that for quadrotors the gyroscopic terms produced by the propeller are dominant with respect to the angular-rate terms. This is a consequence of the high rotational speed Ω.

Simulation Results and Experimental Flight Tests

Some numerical simulations are performed to validate the mathematical model. Hovering flight has to be considered as a reference condition. Thus, the Euler angles and the angular velocities should remain close to zero.

Figs. 8 and 9 represent the platform response when no feedback control is applied. As previously mentioned, the quadrotor is unstable if a perturbation is imposed without a controller. The minimum requirement for acceptable flying qualities is that the platform must be stable after a given disturbance (prerequisite), demonstrating a tendency to return to its initial attitude. To reproduce the controller-board behavior and to validate the model, a PD controller is set. The final gain scheduling (Table 2) is obtained with a trial-and-error method.

The feedback on the yaw angle and rate is not considered. In Figs. 10 and 11, after an oscillatory trend in the first seconds after the perturbation, the platform can stabilize a hovering flight, with null angular velocities and Euler angles. As visible in Fig. 10, the vehicle tends to bank to the right before obtaining the initial position because of the platform lateral instability.

If the same gain scheduling is uploaded on the controller board and hover flight is experimentally reproduced, the results are as shown in Figs. 12 and 13. Because of the structural vibrations and derivation noise, the two responses appear to be comparable considering the general trends, even if further improvement of the controller performance is advisable.

The Euler angles have a rise time of about 10 s, which is not adequate for a platform of these dimensional and dynamic characteristics. For the roll angular rate without a filter on the feedback signal, a maximum overshoot of about 10 rad/s is reached because of the aforementioned numerical evaluation (a second-order finite-difference formula). A low-pass filter should be implemented to avoid numerical noise.

The results obtained are not thorough enough because of the slow response when a perturbation has occurred on the platform. For this reason a new controller board is designed to address the implementation of different control laws.

Dynamic Analysis and Eigenstructure Assignment

To implement the controller, the equations of motion are expressed in the state-space form, deriving linear constant-coefficient state and output equations. The quadrotor dynamic stability was analyzed in hovering flight.

The stability derivatives are usually presented as the ratio of the force changes normalized with the aircraft mass or the moment changes with respect to the appropriate moment of inertia (Prouty 2005). This approach provides derivatives that can be compared with respect to the magnitude from one aircraft to another, even if they vary widely in size. In the case of hover, the derivatives can be assumed in simplified form.

The static stability derivative is denoted by M_w, and it represents the change in pitching moment about the aircraft center of mass when the platform is subject to a perturbation in normal velocity w or in incidence. If M_w is positive, then the aircraft is said to be statically unstable; if M_w is negative, then the aircraft is statically stable

J. Aerosp. Eng. 2012.25:559-573.

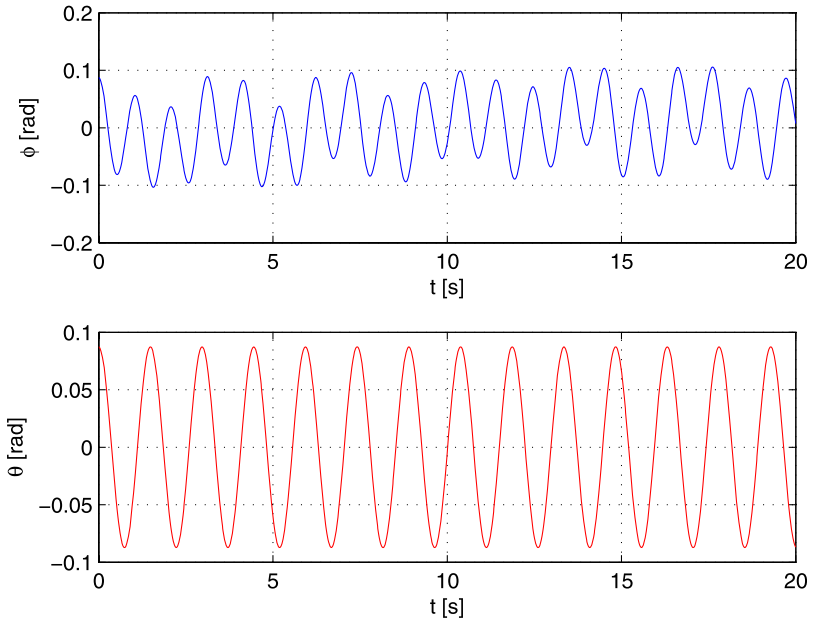

Fig. 8. Trend of the Euler angles without feedback

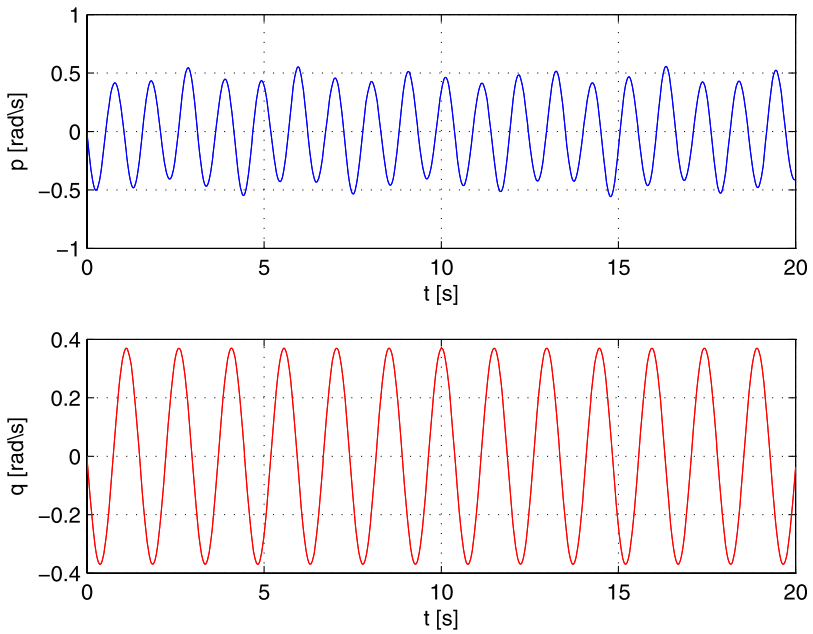

Fig. 9. Trend of the roll and pitch rates with no feedback

Table 2. Gain Scheduling

Parameter	Gain
Proportional controller	
ϕ gain	−1.6
θ gain	−0.6
PD controller	
ϕ gain	−0.8
θ gain	−1.2
p gain	−0.2
q gain	−0.8

(Padfield 2007). For a quadrotor, this parameter is configuration dependent. The coupled pitch-heave motion is an approximation for a multirotor UAV and has a limited range of application because of the coupling of the modal response with speed variations, largely reflected in the speed derivative M_u. This speed derivative is significant even in the hovering condition, and it can contribute to the dynamic instability of the phugoid mode (Padfield 1981). In hover $M_w = 0$, so the pitch and heave motions are uncoupled, giving first-order transients. (The decay rate is given by the derivatives Z_w and M_q.)

For a controller, the cross-coupling derivatives are evaluated, and the assumption of decoupled planes has to be dropped.

A desirable property of a system is that the system poles including feedback should be insensitive to perturbations; this

J. Aerosp. Eng. 2012.25:559-573.

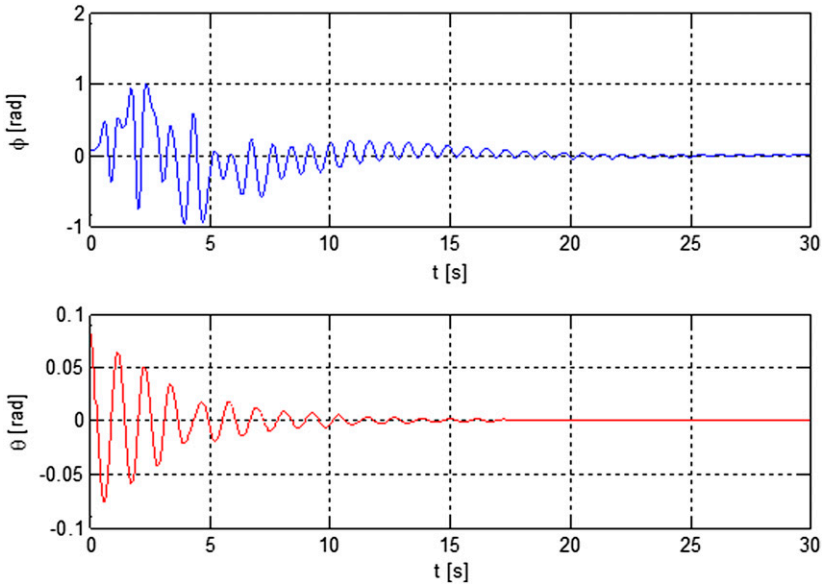

Fig. 10. Variation of the Euler angles with a PD controller

criterion is considered to produce a well-conditioned or robust solution (Kautsky et al. 1985). The feedback matrix is obtained by assigning linearly independent eigenvectors as well conditioned as possible. The system behavior in the state-space formulation is governed by the system poles.

The pole placement has been made considering the desired dynamic specifications, that is:

- Slow response for the vertical speed obtained with the concurrent variation of the four rotational speeds;
- Similar trend for the pitch and roll rate; and
- Fast response for the yaw rate.

Remember that the response on the yaw axis is unstable, and it is characterized by a fast trend. The vertical speed and the yaw rate are not coupled like the roll and pitch rates. Thus two real eigenvalues and a couple of complex conjugates are chosen. The roll and pitch modes have the same behavior, and the heave dynamics can be slower than the other control parameters. The yaw control variable has to be the fastest.

L1 Adaptive Controller

There are many reasons why researchers prefer adaptive laws to find control signals, especially for nonlinear problems for which an analytical solution is barely possible. Uncertainties in the system, disturbances, and measurement noise are some of these reasons. The L1 adaptive strategy was recently introduced by Cao and Hovakimyan (2006a, b). This new approach presents better results, especially during the transient phase. It can provide robust performance against external disturbances and measurement noises. Some advantages of the L1 adaptive architecture are the improved asymptotic tracking and the guaranteed time-delay margin, achieved via smooth control input.

The L1 adaptive control approach replaces the conventional model-reference adaptive control by first specifying an equivalent model architecture, which enables an insertion of a low-pass filter in the closed-loop system. Without a low-pass filter the reference signal, including the high-frequency component, is passed exactly to the control channel. The filter is introduced with the understanding that uncertainties in any feedback loop can only be compensated for within the bandwidth of the control channel. The decoupling between fast adaptation and robustness, inherent to all L1 adaptive control architectures, is achieved via the introduction of this low-pass filter on the adaptive control signal. This feature permits one to avoid high-frequency oscillations because of the large adaptation gain; in systems that use electric devices these oscillations significantly increase the current draw, which is undesirable.

The L1 adaptive control theory's systematic design procedures also significantly reduce the tuning effort required to achieve the desired closed-loop performance, particularly while operating in the presence of uncertainties and failures.

The elements of the L1 adaptive controller are the state predictor, the adaptive law, and the control law. The state predictor is defined similarly to the plant equations, by replacing the unknown variables with their estimates. The adaptive controller is based on a piecewise constant adaptive law and defines a state predictor to estimate the uncertainties (Xargay et al. 2010). The adaptive algorithm ensures uniformly bounded transient response for the system's inputs and outputs, simultaneously, in addition to steady-state tracking.

The problem formulation is

$$\begin{cases} \dot{\mathbf{x}}(t) = \mathbf{A}_m\mathbf{x}(t) + \mathbf{B}_m\mathbf{K}_g\mathbf{u}(t), & \mathbf{x}(0) = \mathbf{x}_0, \\ \mathbf{y}(t) = \mathbf{C}x(t) \end{cases} \tag{15}$$

where $\mathbf{x}(t)$ = system state vector, $\mathbf{u}(t)$ = control signal, $\mathbf{y}(t)$ = regulated output, $\mathbf{A}_m$ = known Hurwitz matrix that defines the desired dynamics for the closed-loop system, and $\mathbf{B}_m$ and $\mathbf{C}$ = known constant matrices.

Assumption 1

There exists a control matrix $\mathbf{K}_n$ such that $\mathbf{A}_m = \mathbf{A} - \mathbf{B}\mathbf{K}_n$ is Hurwitz. The matrix $\mathbf{K}_n$ is calculated from the pole-placement theory (Kautsky et al. 1985).

The control objective is to design an adaptive state feedback controller to guarantee that the output $\mathbf{y}(t)$ tracks the response of a desired system $\mathbf{M}(s) \equiv \mathbf{C}(s\mathbf{I}-\mathbf{A}_m)^{-1}\mathbf{B}_m\mathbf{K}_g(s)$, where $\mathbf{K}_g(s)$ is a feedforward prefilter. This filter is a constant matrix where the diagonal elements of the desired transfer matrix $\mathbf{M}(s)$ have gain at zero

J. Aerosp. Eng. 2012.25:559-573.

frequency (DC gain) equal to 1, while the off-diagonal elements have zero DC gain.

The prefilter $\mathbf{K}_g(s)$ can be calculated starting from matrices $\boldsymbol{A}_m$ and $\boldsymbol{B}_m$ as follows:

$$\mathbf{K}_g(s) \equiv \mathbf{K}_g = -(\mathbf{C}\mathbf{A}_m^{-1}\mathbf{B}_m)^{-1} \tag{16}$$

The state predictor can be written as

$$\dot{\hat{\mathbf{x}}}(t) = \mathbf{A}_m\hat{\mathbf{x}}(t) + \mathbf{B}_m\big(\mathbf{u}(t) + \hat{\boldsymbol{\sigma}}_m(t)\big) \tag{17}$$

where $\mathbf{B}_m = \mathbf{B}$ because only the hover maneuver has been considered and $\hat{\boldsymbol{\sigma}}_m(t)$ = vector of matched eigenvalues.

The adaptation law for $\hat{\boldsymbol{\sigma}}_m(t)$ is defined as

$$\hat{\boldsymbol{\sigma}}_m(t) = -\mathbf{B}^{-1}\boldsymbol{\Phi}(T_s)\exp^{\mathbf{A}_m T_s} \tag{18}$$

where T_s = the sampling time and $\boldsymbol{\Phi}(T_s)$ is a square matrix given by

$$\boldsymbol{\Phi}(T_s) = \mathbf{A}_m^{-1}\left(\exp^{\mathbf{A}_m T_s} - I_n\right) \tag{19}$$

As a final step, the control law is considered. The control signal is the output of the following system:

$$\begin{cases} \mathbf{u}(t) = -\mathbf{K}_n\mathbf{D}(s)\hat{\boldsymbol{\eta}}(s), \\ \hat{\boldsymbol{\eta}}(t) = \mathbf{u}(t) + \hat{\boldsymbol{\sigma}}_m(t) - \mathbf{r}_g(t) \end{cases} \tag{20}$$

where $\mathbf{D}(s)$ = identity matrix and $\mathbf{r}$ = reference signal.

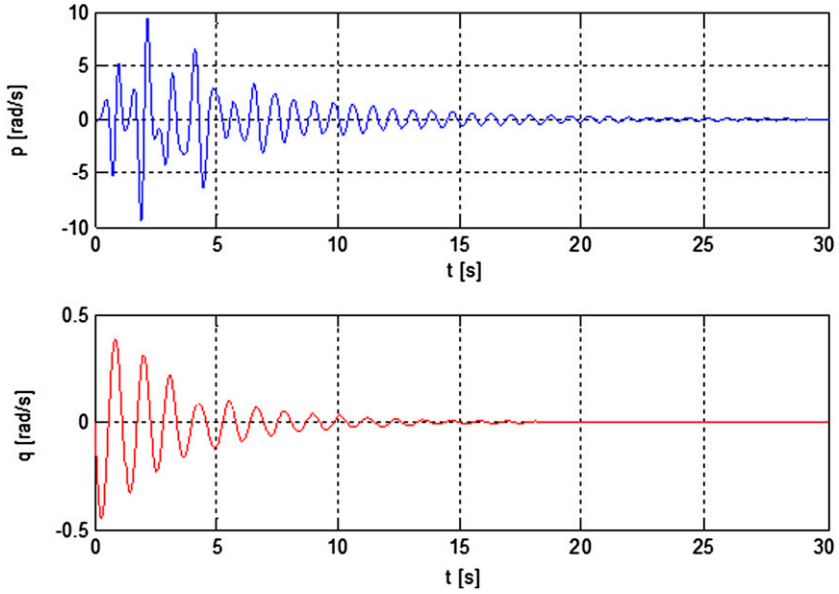

Fig. 11. Angular-velocity variation with a PD controller

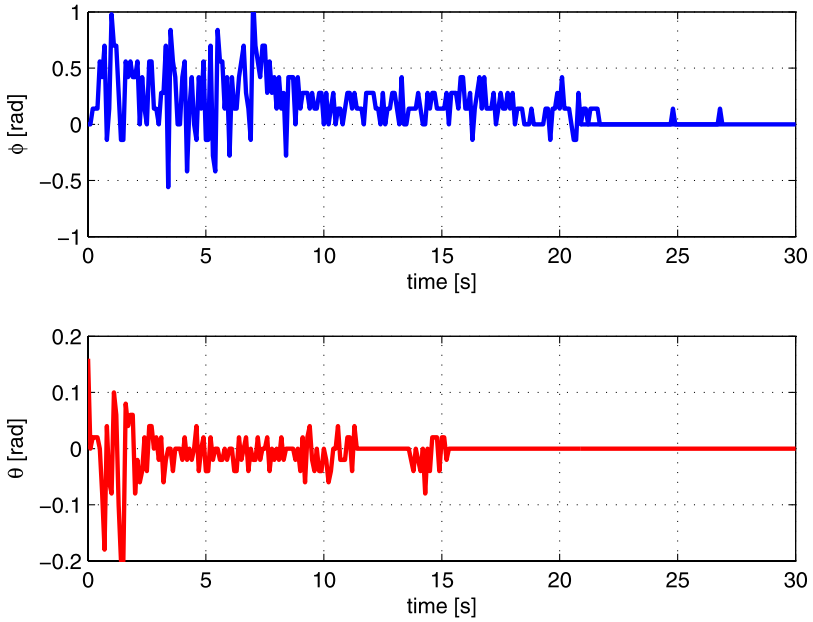

Fig. 12. Experimental trend of the roll and pitch angles

J. Aerosp. Eng. 2012.25:559-573.

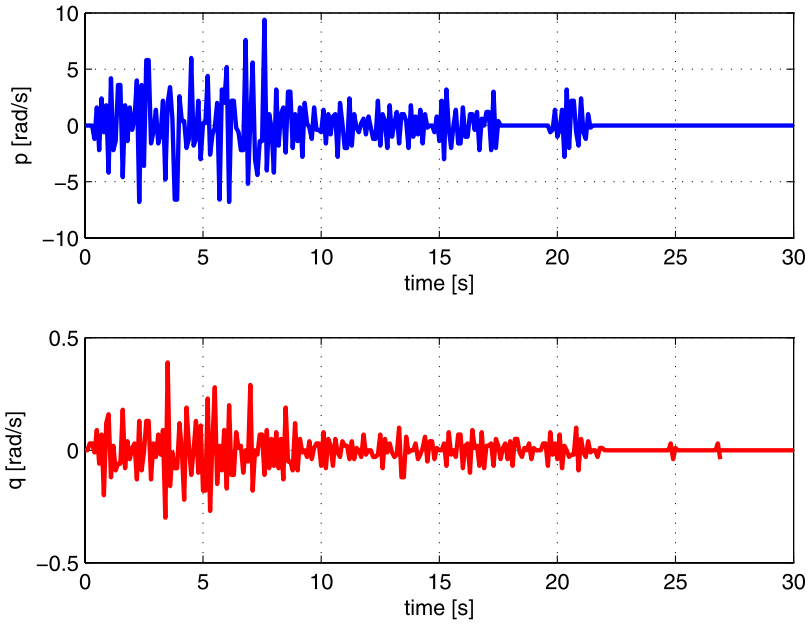

Fig. 13. Experimental trend of the roll and pitch angular velocities

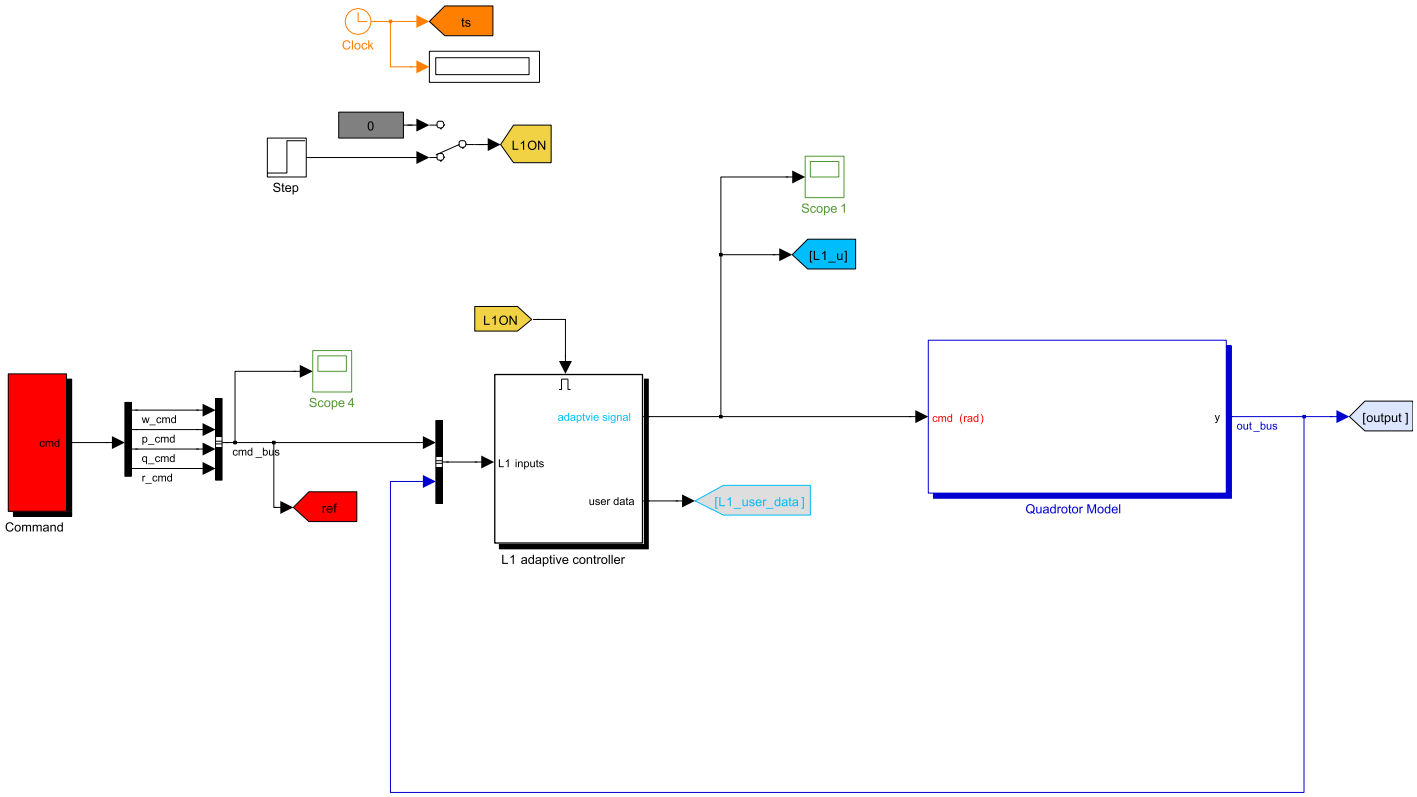

Fig. 14. Simulink model including the L1 adaptive controller

In the control-law block, a low-pass filter with high bandwidth has to be modeled to guarantee an adequate robustness margin. With this filter the system becomes less susceptible to measurement noise; this is fundamental for a platform like a quadrotor.

The simulation scheme is visible in Fig. 14. Setting as a reference a doublet maneuver for the p and q variations, a step for the yaw angular velocity, and a vertical hold speed (corresponding to the hovering), the simulation results have been reported in Figs. 15–18.

As shown in Fig. 19 a change in the pitch rate generates a variation of the rotational speeds related to the roll axis (Ω_2 and Ω_4) because of the coupling between these two control variables. This coupling is smaller for the opposite command (perturbation on the roll rate) because of the entity of the coupling derivatives in the state

J. Aerosp. Eng. 2012.25:559-573.

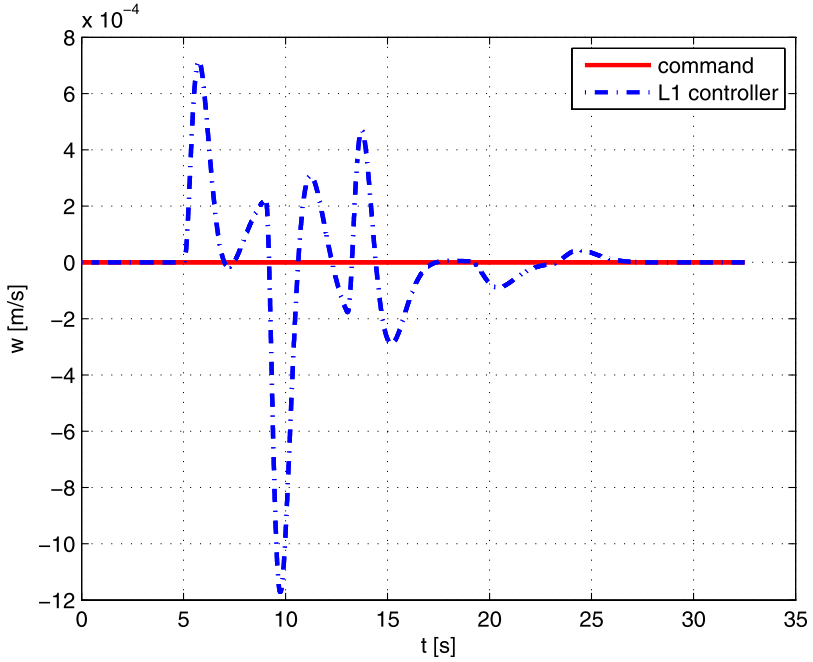

Fig. 15. Variation of the vertical speed

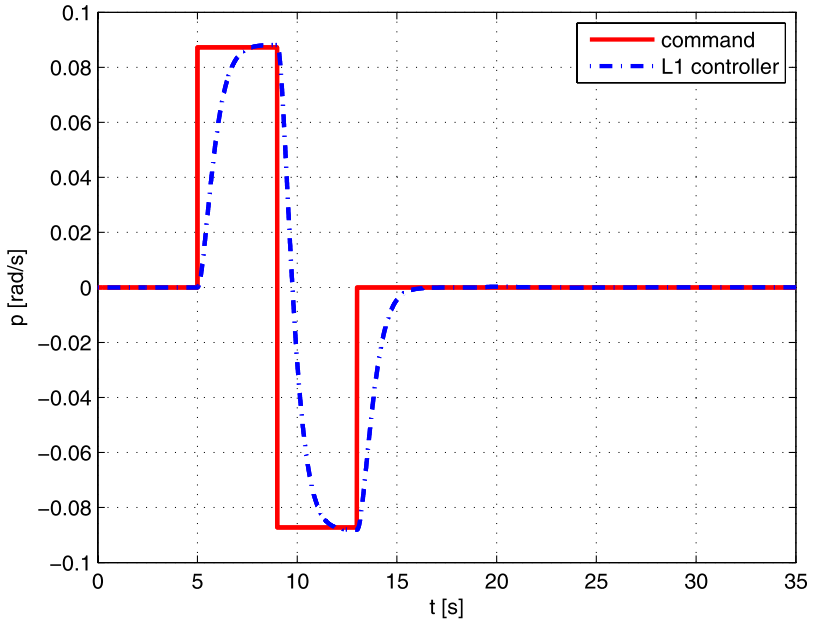

Fig. 16. Trend analysis of roll angular rate

matrix. As a matter of fact, the derivative L_q has a greater value than M_p.

After 5 s, a roll command is assigned, this causes a variation on the even rotors and a small variation on the odd ones. If a perturbation on the pitch rate is assigned after 15 s, the large variation can be noted in the odd motors, but the coupling causes a variation also in the other two motors. The yaw is obtained by varying the four motors.

With the L1 controller the platform can perform a fast maneuver along the three axes, even if there are small oscillations in the vertical speed. The controller is implemented in hover, but, using a gain scheduling on the speed variation, the model can be implemented in different flight conditions, without the tuning of the model matrices (Kharisov et al. 2008). The responses can be improved with a different pole placement, but the actuator characteristics and the system performance have to be modeled with accuracy.

Conclusion

In the Aerospace Engineering Department of Politecnico di Torino, a quadrotor is under development for territorial-monitoring applications and as a flying test bed for different feedback control systems.

J. Aerosp. Eng. 2012.25:559-573.

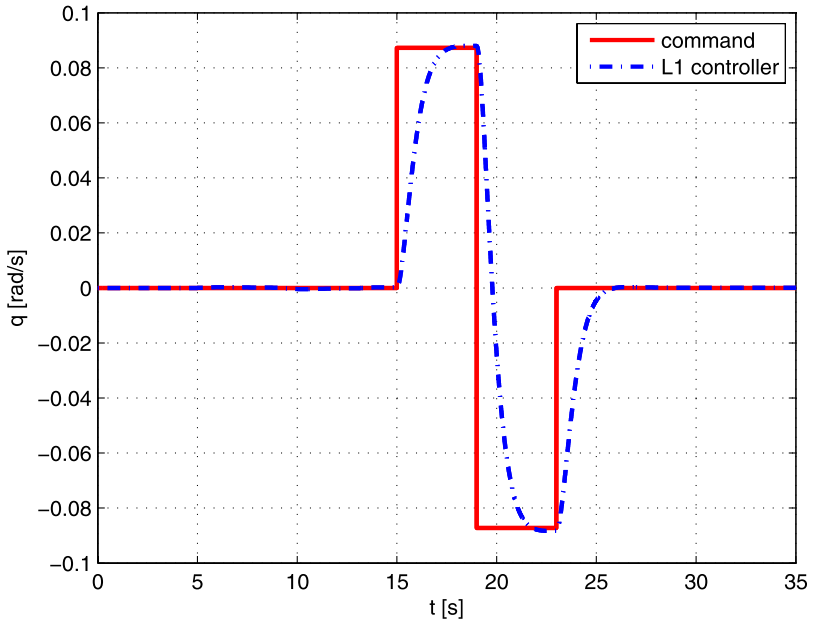

Fig. 17. Pitch angular rate trend

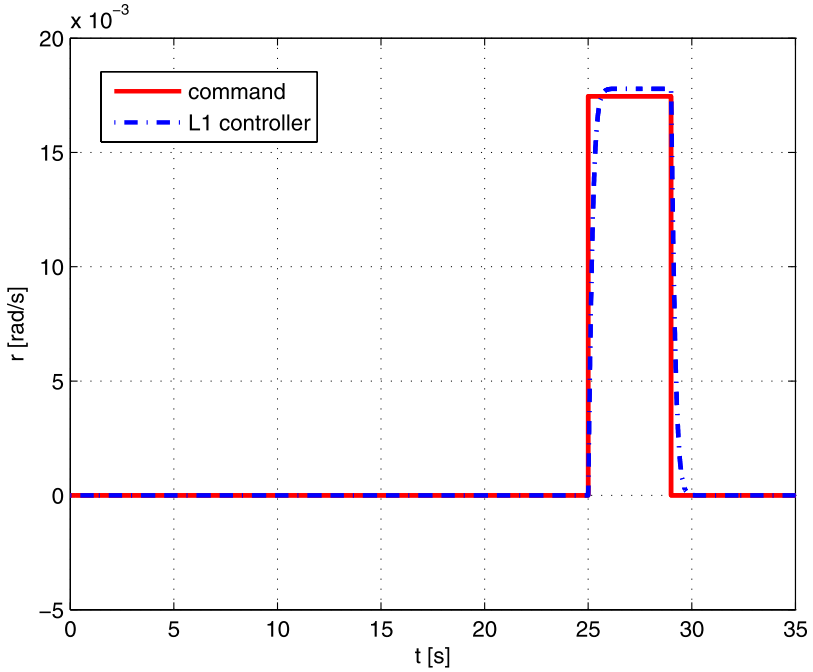

Fig. 18. Variation of the yaw angular rate

Some experiments have been carried out with a PD controller to validate the developed mathematical model, and they demonstrated that, except for noise because of structural vibration, the simulations performed in Matlab/Simulink partially matched the real behavior of the quadrotor. The response is dynamically stable, and after a perturbation, the aircraft is moving to the equilibrium point.

To enhance the response of the vehicle and to cancel the derivation noise, some simulations with an L1 controller have been carried out, but it has not been yet possible to verify experimentally if the controller works as expected.

The philosophy of an L1 controller is to introduce separation between adaption and robustness. This controller defines the control signal as the output of a low-pass filter to guarantee that the control signal stays in the low-frequency range. The controller state matrix is based on the pole-placement theory, and it is possible to demonstrate that the adaptive controller is applicable in different flight operations with the same gain matrix.

The next step includes the validation of the stability characteristics in remote control. It can be demonstrated that the gain matrix $\mathbf{K}_n$ and the adaptive algorithm are compatible, and it is possible to verify if the simulation results are similar to the experimental data.

J. Aerosp. Eng. 2012.25:559-573.

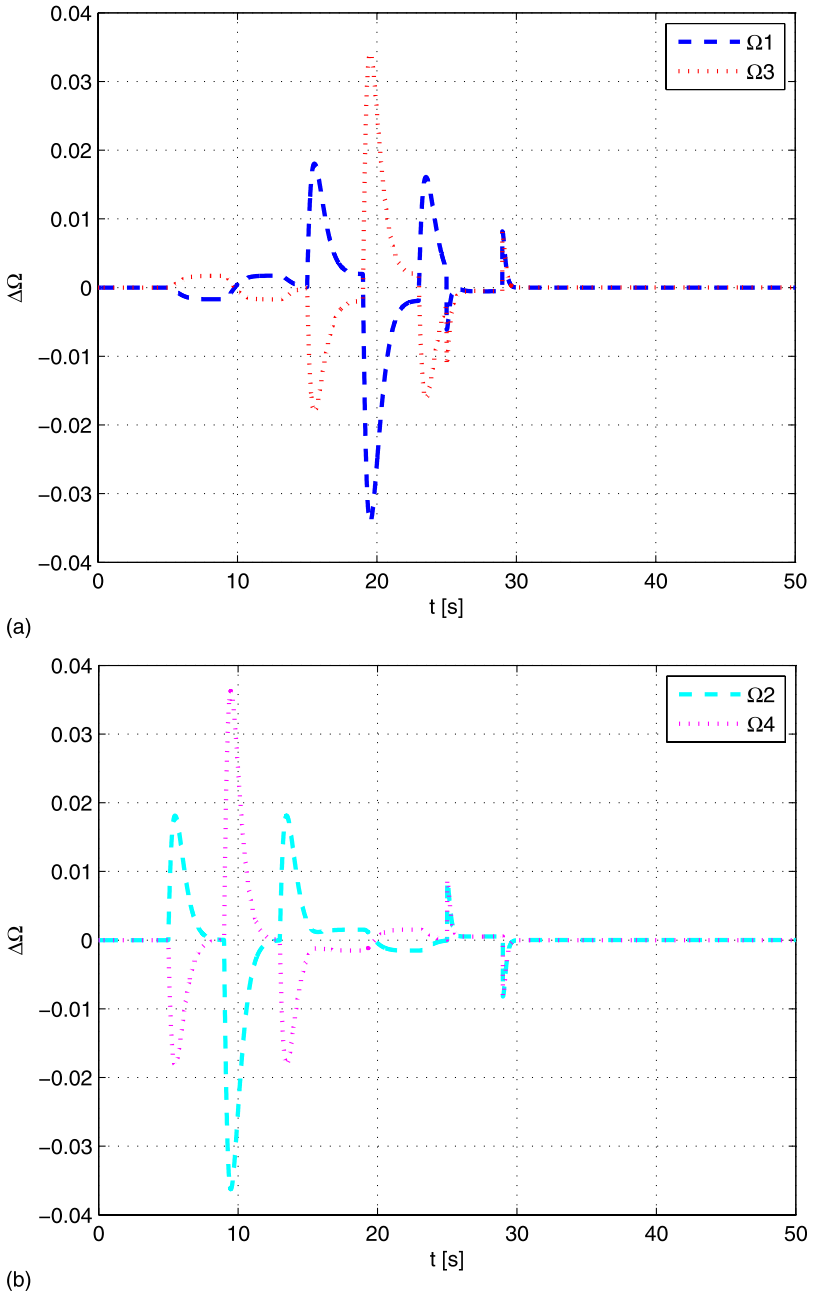

Fig. 19. Variation of the four rotational speeds

A new controller board will be designed, implementing an L1 customized control algorithm. Moreover, the implementation of an L1 controller in the autopilot can reduce the measurement noise. The low-pass filter in the control law can also be useful for improving the data acquisition of the accelerometers and for the flight tests combined with the Kalman filter (to have less noisy results). This combined solution detects a new steady state and uses the Kalman filter model to estimate and correct the attitude. Thus, this auto-correction property permits one to avoid any estimation bias.

Acknowledgments

The authors thank Professor Naira Hovakimyan and her group at the University of Illinois at Urbana-Champaign for sharing experience and knowledge on the L1 controller theory and implementation.

Notation

The following symbols are used in this paper:

$\mathbf{A}_m$ = pole-placement matrix for L1 controller;
a_p = acceleration of a point along blade;
$\mathbf{B}_m$ = control matrix for L1 controller;
$\mathbf{C}$ = output matrix;
C_D = blade drag coefficient;
CG = center of gravity;
C_i = torque on ith propeller;
C_L = blade lift coefficient;
c = chord of blade;
dD = infinitesimal drag;
dL = infinitesimal lift;
dm = infinitesimal mass of blade;

J. Aerosp. Eng. 2012.25:559-573.

g = acceleration of gravity;
I_X, I_Y, I_Z = moments of inertia along x-, y-, z-axes, respectively;
$\mathbf{K}_g$ = feedforward prefilter;
M_w = stability static derivative;
p, q, r = roll, pitch, and yaw angular velocities, respectively;
R = rotor radius;
$\mathbf{R}^i_j$ = transformation matrix from ith frame to jth frame;
r_0 = moment arm;
T_i = thrust on ith propeller;
T_s = sampling time;
U_0 = asymptotic air speed;
w = speed along z body axis;
β = constant blade flapping angle;
ζ = constant lag flapping angle;
λ = inflow;
θ, φ, ψ = Euler angles;
ρ = air density;
$\hat{\boldsymbol{\sigma}}_m$ = vector of matched eigenvalues;
χ = angle between asymptotic air speed and Y_2 axis;
Ψ = azimuth angle; and
Ω_i = propeller angular velocity.

References

Cao, C., and Hovakimyan, N. (2006a). "Design and analysis of a novel L1 adaptive control architecture, Part 1: Control signal and asymptotic stability." *Proc., 2006 American Control Conf.*, IEEE Conference Publishing, Washington, DC, 3397–3402.

Cao, C., and Hovakimyan, N. (2006b). "Design and analysis of a novel L1 adaptive control architecture, Part 2: Guaranteed transient performance." *Proc., 2006 American Control Conf.*, IEEE Conference Publishing, Washington, DC, 3403–3408.

Capello, E., Guglieri, G., and Quagliotti, F. (2009). "A design configuration and optimization for a multi rotor UAV." *NATO RTO Symp. Intelligent Uninhabited Vehicle Guidance Systems,* North Atlantic Treaty Organization, Brussels, Belgium, 31.

Castillo, P., Dzul, A., and Lozano, R. (2004). "Real-time stabilization and tracking of a four-rotor mini rotorcraft." *IEEE Trans. Contr. Syst. Technol.*, 12(4), 510–516.

Etkin, B., and Reid, L. (1995). *Dynamics of flight: Stability and control*, Wiley, New York.

Flachsbart, O., and Krober, G. (1929). "Experimental investigation of aircraft propellers exposed to oblique air currents." *NACA-TM-562*, National Advisory Committee for Aeronautics, Washington, DC.

Guernard, N., Hamel, T., and Moreau, V. (2005). "Dynamic modelling and intuitive control strategy for an X4 flyer." *Proc., Int. Conf. on Control and Automation,* IEEE Conference Publishing, Washington, DC, 141–146.

Johnson, W. (1994). *Helicopter theory*, Dover, New York.

Kautsky, J., Nichols, V., and Van Dooren, P. (1985). "Robust pole assignment in linear state feedback." *Int. J. Control*, 41(5), 1129–1155.

Kharisov, E., Gregory, I., Cao, C., and Hovakimyan, N. (2008). "L1 adaptive control law for flexible space launch vehicle and proposed plan for flight test validation." *Proc., AIAA Guidance, Navigation and Control Conf.,* American Institute of Aeronautics and Astronautics, Reston, VA, 7128.

Lynn, A., and Fuerst, W. (1995). *Introductory digital signal processing with computer applications*, Wiley, Chichester, U.K.

McKerrow, P. (2004). "Modeling the Draganflyer four-rotor helicopter." *Proc., IEEE Int. Conf. on Robotics and Automation.* IEEE Conference Publishing, Washington, DC, 3596–3601.

Padfield, G. (1981). "On the use of approximate models in helicopter flight mechanics." *Vertica*, 5(1), 243–259.

Padfield, G. (2007). *Helicopter flight dynamics: The theory and the application of flying qualities and simulation modelling*, Blackwell, Oxford, U.K.

Pamadi, B. (2004). *Performance, stability, dynamics and control of airplanes*, American Institute of Aeronautics and Astronautics, Reston, VA.

Pounds, P., Mahony, R., Hynes, P., and Roberts, J.(2002). "Design of a four-rotor aerial robot." *Proc., Australian Conf. on Robotics and Automation,* Australian Robotics and Automation Association, Sydney, Australia, 145–150.

Prouty, R. (2005). *Helicopter performance, stability and control*, Krieger, Malabar, FL.

Stevens, B., and Lewis, F. (2003). *Aircraft control and simulation*, Wiley, New York.

Xargay, E., Hovakimyan, N., and Cao, C. (2010). "L1 adaptive controller for multi-input multi-output systems in the presence of nonlinear unmatched uncertainties." *Proc., 2010 American Control Conf.,* IEEE Conference Publishing, Washington, DC, 874–879.